UNIVERSITY OF CALIFORNIA, SAN DIEGO

# INTRUSIVE GRAVITY CURRENTS

A Thesis submitted in partial satisfaction of the requirements for the degree Master of Science

in

Chemical Engineering

by

Alice Thanh Hang

Committee in Charge:

Professor Paul Linden, Chair
Professor Stefan Llewellyn Smith
Professor Sutanu Sarkar

2009

The thesis of Alice Thanh Hang is approved and it is acceptable in quality and form for publication on microfilm and electronically:

_____

_____

_____

Chair

University of California San Diego

2009

TABLE OF CONTENTS

LIST OF FIGURES

LIST OF TABLES

ACKNOWLEDGEMENTS

I would like to acknowledge Professor Paul F. Linden, the chair of my committee, whose guidance and support helped me with my research at the University of California San Diego. I would also like to acknowledge the help of Diogo Bolster, Morris Flynn, and Thomas Boubarne for helping me conduct experiments necessary to complete my research. As for my remaining committee members, Professors Sutanu Sarkar and Stefan G. Llewellyn Smith, I would like to thank them for being a positive experience during my time at the university.

Chapter 4 in part has been published in the *Journal of Fluid Mechanics*, 2008, D. Bolster., A. Hang, and P.F. Linden. **594**. pp. 369-377 (Cambridge University Press). I was an investigator in the paper written above.

ABSTRACT OF THE THESIS

Intrusive Gravity Currents

by

Alice Thanh Hang

Master of Science in Chemical Engineering

University of California, San Diego, 2009

Professor Paul F. Linden, Chair

This thesis will discuss equilibrium and non-equilibrium intrusive gravity currents or intrusions, in two layer and continuous stratifications. Although the associated time and length scales are significantly smaller than those appropriate to most natural flows of interest, insights can occur when discussing actual laboratory experiments provided that the Reynolds number is sufficiently large so that viscous effects do not show a leading order influence. Lock release experiments were performed and the speed was analyzed using DigImage and Digiflow. The equilibrium intrusion is

discussed which is an extension of the doubly symmetric case, where the density of the current is the depth-weighted mean density of the layers. The non-equilibrium case is also discussed and unlike the equilibrium flow, the intrusion fluid steadily rises or falls behind the intrusion front, adding an additional source of energy to drive the flow. These intrusions were performed in two-layer and continuous stratifications. The results presented in this thesis include experimental and numerical data and follow closely to the work of previous researchers' theoretical models.

# *Chapter 1*

# THESIS OUTLINE AND SCOPE

## 1.1 Introduction

Intrusive gravity currents arise when a fluid of intermediate density intrudes into a stratified fluid. These intrusions may occur in both natural and human-made settings and may be the results of a sudden release of a fixed volume of fluid or a time-dependent addition of such a fluid. After reviewing previous work on the related topic of gravity currents, experimental results of interfacial intrusions and continuous stratification intrusions will be discussed.

The first quantitative study of gravity currents was performed by Von Karman in 1940. Using Bernoulli's theorem, Von Karman showed that the velocity, $U$, of the nose followed by a layer of depth $h$ of relatively heavy fluid of density $\rho_i$ in a fluid of density where $\rho_0 < \rho_i$ was given by

$$U / (g_{iU}\, 'h)^{1/2} = Fr, \qquad (1.1)$$

where the reduced gravity $g_{iU}\, ' = g(\rho_i - \rho_U)/\rho_0$, where g is the acceleration due to gravity and the Froude number, $Fr$, was evaluated by Von Karman to be $\sqrt{2}$. The Froude number is the only non-dimensional parameter that can be constructed from the characteristics of the steady current $U$, $g'$, and $h$ at high Reynolds number, $Re$. This is the condition that has generally

been applied at the nose of a current propagating into a very deep ambient at high Reynolds number $Re = Uh/\nu$, where $\nu$ is the kinematic viscosity of the ambient.

Since then other researchers (Benjamin (2), Simpson & Britter (5) and others) have revisited this problem and (1.1) has been used in almost all studies of gravity currents at high Reynolds numbers as a form of conservation of momentum but with different values of *Fr*. In almost all situations a current whose density difference is due to a dissolved component of negligible diffusivity, such as salt, acts in such a way that its horizontal extent is much larger than its vertical one. If the Reynolds number is large, the balance between inertial and buoyancy forces can be applied, as well as shallow water theory

Gravity currents and internal gravity waves are present in the atmosphere and ocean. Atmospheric examples include thunderstorm outflows and sea breeze fonts (Simpson (20), (21)). Internal gravity waves, which propagate within density stratified environments, play an important role in atmospheric circulation. For example, in the breakdown of internal gravity waves conveys a significant drag on the zonal winds (Becker & Schmitz (4)). Although the largest proportion of momentum transport by internal gravity waves is associated with those generated by topographic forcing (Fritts & Nastrom (9)), other dynamic excitation mechanisms can also result in significant momentum fluxes.

Internal waves in natural flows may be generated by a number of different mechanisms. Internal waves are generated by the passage of the current. Depending on the speed, they can be supercritical that flow downstream or subcritical that flow upstream and downstream. But although they can carry momentum and energy, they do not affect the speed of the current when the current's density is greater than the maximum density of the ambient fluid. These propagate at the lower boundary of the domain and are gravity currents. An intrusion flows between the extremes of the ambient fluid density, and propagates along an isopycnal surface.

## 1.2 Hydraulic Theory

### 1.2.1 Benjamin's Theory for Gravity Currents

Benjamin (2) proposed a hydraulic theory for gravity currents that flow in a channel along a solid horizontal boundary. This theory discusses a relationship between the front speed and downstream depth of the current based on mass and momentum. The theoretical speed, $U$, of a gravity current of density $\rho_i$ propagating into an ambient fluid of density $\rho_0 < \rho_i$ and finite depth $h_T$ is given implicitly by

$$\frac{U^2}{g' \Delta d} = \frac{(h_T - \Delta d)(2 h_T - \Delta d)}{h_T (h_T + \Delta d)} \tag{1.2}$$

in which $\Delta d$ is the depth of the trailing tail sufficiently far behind the head and $g'$ is the reduced gravity. Here, we have invoked the Boussinesq approximation so the density difference $\rho_L - \rho_0$ is normalized by a characteristic density $\rho_{00}$.

There are two limits of interest. For energy-conserving currents, $\Delta d = h_T/2$ and so (1.2) gives

$$U \rightarrow \sqrt{(g' \, \Delta d / 2)}. \tag{1.3}$$

In the limit $h_T >> \Delta d$, energy cannot be conserved in the context of Benjamin's theory. Nonetheless, the speed can be predicted by the equation

$$U \rightarrow \sqrt{(2g' \, \Delta d)}. \tag{1.4}$$

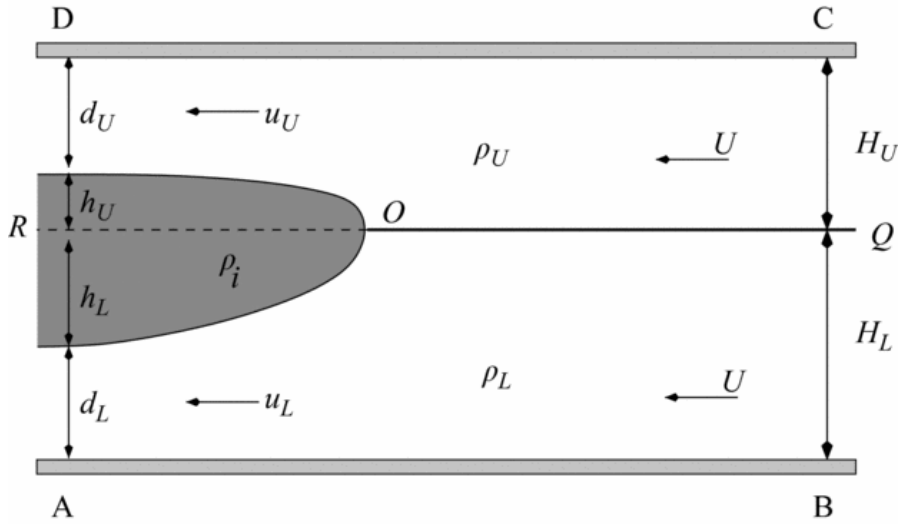


**FIGURE 1.1** Sketch of an intrusion (shaded) and the control volume ABCD. The frame reference is chosen so that the intrusion is at rest.

### 1.2.2 Intrusions in a Two-Layer Fluid

Holyer & Huppert (10) extended the theory of Benjamin (2) to intrusions propagating in a two-layer fluid. We consider an intrusion of density $\rho_i$ moving along an interface between upper and lower layers of respective depths $H_U$ and $H_L$, and where z=0 corresponds to the height of the interface and $p_Q$ is the pressure along the interface far upstream from the intrusion. Along the vertical segment BC,

$$p = \begin{cases} p_Q - g\ \rho_U\ z, & 0 < z < H_U, \\ p_Q - g\ \rho_L\ z, & -H_L < z < 0, \end{cases} \tag{1.5}$$

where $\rho_U$ is the upper layer density and $\rho_L$ is the lower layer density, and $g$ is the gravitational acceleration. Along the vertical AD,

$$p = \begin{cases} p_R - g\rho_i\ h_U - g\ \rho_U(z - h_U), & h_U < z < H_U, \\ p_R - g\rho_i\ z, & 0 < z < h_U, \\ p_R - g\rho_i\ z, & -h_L < z < 0, \\ p_R + g\rho_i\ h_L - g\rho_L\ (z + h_L), & -H_L < z < -h_L, \end{cases} \tag{1.6}$$

where $h_U$ and $h_L$ represent the vertical distances of the intrusion shown in Figure 1.1. In this figure, the pressure of the stagnation point is $P_R = P_O$ and the fluid inside is at rest.

Since it is assumed that energy is conserved along streamlines in the flow, we can apply Bernoulli's equation. Therefore, along the lower boundary of the intrusion downstream from the stagnation point, we find

$$u_L^2 = 2g'_{Li}\, h_L = 2g'_{Li}\,(H_L - d_L), \qquad \text{where} \qquad g'_{Li} \equiv g\frac{\rho_L - \rho_i}{\rho_0} \tag{1.7}$$

is the reduced gravity of the intrusion where $\rho_0$ is a characteristic density. A similar relation to (1.7) holds for the upper layer.

Shown in Figure 1.1, are the layer depths, $d_U$ and $d_L$ and are given by

$$d_U = \frac{U\ H_U}{u_U}, \qquad d_L = \frac{U\ H_L}{u_L}. \tag{1.8}$$

Conservation of mass therefore gives us, from (1. 7) and (1.8),

$$g'_{iU}\frac{(H_U - d_U)\ d_U^2}{H_U^2} = g'_{Li}\frac{(H_L - d_L)\ d_L^2}{H_L^2}. \tag{1.9}$$

An independent relation for $d_U$ and $d_L$ can be obtained from horizontal momentum conservation in the control volume ABCD. Because there are no external forces imposed, we find

$$\int_A^D p + \rho u^2\, \mathrm{d}z = \int_B^C p + \rho u^2\, \mathrm{d}z. \tag{1.10}$$

Using the hydrostatic pressure distributions (1.5) and (1.6) and the upper and lower layer speeds given by (1.7), we find

$$\begin{aligned}\frac{p_O - p_Q}{\rho_0} H = {} & g'_{iU}\left\{\frac{1}{2}(H_U^2 - d_U^2) - \frac{2d_U}{H_U}(H_U - d_U)^2\right\} \\ & + g'_{Li}\left\{\frac{1}{2}(H_L^2 - d_L^2) - \frac{2d_L}{H_L}(H_L - d_L)^2\right\}.\end{aligned} \tag{1.11}$$

Applying Bernoulli's equation upstream along the interface, a second expression for $p_O - p_Q$ is obtained

$$\frac{p_0 - p_Q}{\rho_0} H = g'_{iU} \frac{d_U^2}{H_U}(H_U - d_U) + g'_{Li} \frac{d_L^2}{H_L}(H_L - d_L). \tag{1.12}$$

Equating 1.11 and 1.12, we get (1.13):

$$g'_{iU} \frac{(H_U - d_U)^2(H_U - 2d_U)}{H_U} + g'_{Li} \frac{(H_L - d_L)^2(H_L - 2d_L)}{H_L} = 0. \tag{1.13}$$

These equations were first derived by Holyer & Huppert (10) and written in this way by Sutherland *et al.* (22) and Flynn & Linden (8). This thesis will discuss equilibrium and non-equilibrium intrusions in two layer and continuous stratifications. Although the associated time and length scales are significantly smaller than those appropriate to most natural flows of interest, insights can occur when discussing actual laboratory experiments provided that the Reynolds number is sufficiently large so that viscous effects do not show a leading order influence. An equilibrium intrusion in a two-layer stratification, which will be discussed in Chapter 2, is where the intrusion is equal to the depth-weighted mean of the layer densities. This intrusion can be considered as two gravity currents propagating at the same speed. Chapter 3 discusses non-equilibrium intrusions in a two-layer fluid. Chapter 4 discusses intrusive gravity currents that flow in a continuous stratification, causing the gravity current to travel along its level of neutral buoyancy (i.e. the height at which the density of the intrusion is the same as that of the ambient fluid).

*Chapter 2*

# EQUILIBRIUM INTRUSIONS IN TWO LAYER FLUIDS

## 2.1 Introduction

This chapter investigates the flow from an instantaneous release of lock fluid into a two-layer ambient stratification. The first circumstance considered is that of a doubly-symmetric intrusion (see Figure 1.1 for a sketch of an intrusion), for which

$$H_U = H_L \text{ and } \rho_i = \tfrac{1}{2}(\rho_L + \rho_U). \qquad (2.1)$$

The doubly symmetric intrusion can be considered as two equal gravity currents, traveling at the same speed. They are mirror images of each other along the interface. (Figure 2.1) In this case, the theory of Holyer & Huppert (10) predicts that the intrusion occupies one-half the total depth, its speed is one-half the interfacial long wave speed, and the interface ahead of the intrusion remains undisturbed.

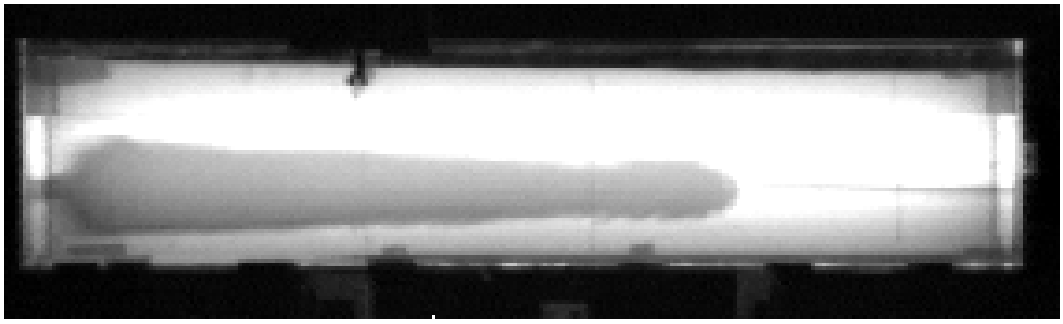

**FIGURE 2.1:** Laboratory experiment of an equilibrium intrusion where $h_E / H = 0.5$.

In this case, the reduced gravity in the lower layer is equal to the reduced gravity in the upper layer, where the reduced gravity is $g' = g(\rho_L - \rho_l)/\rho_{0,}$ where the subscript $L$ indicates the lower layer and $U$ is the upper layer. When an intrusion has a thickness where $h = h_U + h_L = 0$, the intrusion is considered energy conserving for infinitely deep layers ($H_U = H_L \rightarrow \infty$) and $D = H/2$.

Lock release experiments for the doubly-symmetric intrusion were carried out by Britter & Simpson (5). They showed that the interface ahead of the current remained flat and that the current propagates at a constant speed over several lock lengths. An extension of the doubly-symmetric case is the equilibrium intrusion where the density is the depth-weighted mean of the layer densities. This intrusion can be considered as two unequal gravity currents propagating at the same speed. An energy analysis shows that the equilibrium intrusion has the minimum available potential and kinetic energy. Since the two images can be considered mirror images of one another, the equilibrium condition can consider the intrusion is neutrally buoyant with respect to the undisturbed interface such that

$$g'_{IU} h_U = g'_{LI} h_L \tag{2.2}$$

Equation 2.2, where $h_U$ and $h_L$ are the upper and lower layer heights, implies that the upper and lower layer speeds are equal. Flynn & Linden (8) used conservation of mass and momentum to obtain,

$$\frac{d_U}{H_U} = \frac{d_L}{H_L} \Rightarrow d_L + d_U = \frac{1}{2} H \tag{2.3}$$

This equation also shows that the intrusion occupies half the channel depth. The neutral buoyancy condition (2.2) can be written as

$$\rho_i = \rho_E \equiv \frac{\rho_U H_U + \rho_L H_L}{H} \tag{2.4}$$

because (2.3) implies $h_U / H_U = h_L / H_L$,

When the intrusion density is the depth weighted mean density $\rho_E$, a solution can be determined by mass, momentum, and energy equations where the interface remains undisturbed ahead of the intrusion (Sutherland *et al.* (22)). If the intrusion and both layer densities are given, the equilibrium depth, is defined by

$$\hat{h}_E \equiv \frac{h_E}{H} = \frac{g'_{iU}}{g'_{LU}}. \tag{2.5}$$

Cheong, Kuenen, & Linden (6) developed an energy model to describe the front speed of an IGC. The IGC results from a release of potential energy stored in the original lock configuration. After it travels along the interface and all the motion has ceased, the intrusion eventually leaves three layers. The available potential energy (APE) $\Delta P$, per unit length of the channel, defined as the difference in potential energy between the initial and final state, is calculated as

$$\Delta P = \frac{1}{2} g\alpha(1-\alpha)(h^2\rho_L + (H^2 - 2hH)\rho_i + (H^2 + 2hH - h^2)\rho_U). \tag{2.6}$$

The minimum value of this APE occurs when $d \Delta P / dH = 0$. Calculating the APE per unit area, *E,* due to the horizontal density difference gives us

$$E = g \int_{-h}^{0} (\rho_L - \rho_i) z \, dz + g \int_{0}^{H-h} (\rho_i - \rho_U) z \, dz \tag{2.7}$$

$$= \frac{1}{2} g (\rho_L - \rho_i) h^2 + \frac{1}{2} g (\rho_i - \rho_U)(H - h)^2. \tag{2.8}$$

From this, the intrusion speed was developed as

$$\hat{U}_h = F \sqrt{\hat{h}^2 - 2\hat{h}\hat{h}_E + \hat{h}_E}. \tag{2.9}$$

To confirm this theory, we performed intrusion experiments to add to the work that Cheong, Kuenen, & Linden (6) previously performed. The results shown are in good agreement with the theory by Cheong, Kuenen, & Linden (6), and the numerical simulations performed by Flynn & Linden (8).

## 2.2 Numerical Solutions

For an intrusion entering two layers of fluid, a useful approximation can be used by applying an analysis similar to Benjamin's analysis of a boundary current in an infinitely deep ambient. We assume the upstream and downstream velocity profiles are assumed to be smooth. Mixing, viscosity, and surface tension are assumed to be absent. The frame of reference chosen is one in which the intrusion is at rest (Figure 1.1). In this frame, the

origin of the vertical coordinate *z* is chosen at the level of the interface far upstream.

Numerical simulations were performed by Flynn & Linden (8). For a Boussinesq fluid, the governing equations are

$$\nabla \cdot \mathbf{u} = 0\,, \tag{2.10}$$

$$\frac{\mathrm{D}u}{\mathrm{D}t} = -\frac{1}{\rho_0}\frac{\partial P}{\partial x} + \nu\,\nabla^2 u\,, \tag{2.11}$$

$$\frac{\mathrm{D}w}{\mathrm{D}t} = -\frac{1}{\rho_0}\frac{\partial P}{\partial z} - \frac{\rho'\,g}{\rho_0} + \nu\,\nabla^2 w\,, \tag{2.12}$$

$$\frac{\mathrm{D}\rho}{\mathrm{D}t} = \frac{\nu}{\mathrm{Sc}}\,\nabla^2 \rho\,, \tag{2.13}$$

where **u** = (*u,w)* is the velocity, *g* is the gravitational acceleration, $\rho_0$ is a characteristic reference density , *P* is the hydrostatically adjusted pressure, *Sc* is the Schmidt number, ρ(*x,z,t*) is the fluid density, ρ' is a perturbation from the average background density and $\frac{D\phi}{Dt} = \frac{\partial \phi}{\partial t} + \mathbf{u}.\nabla\phi$ denotes a material derivative. For the simulations reported here, $\nu$ = 0.01 cm$^2$/s and *Sc* = 1. Although a Schmidt number of 1 is larger than the physical value of salt and leads to a significant overestimation for the diffusivity of salt, this choice is necessary to maintain numerical stability and does not lead to significant chances in the dynamics of the flow (Maxworthy *et al.* (14) and Ungarish & Huppert (23)).

Zero-flux boundary conditions were imposed on the density field at all boundaries. The velocity field satisfied no-normal flow and no-slip conditions at the boundaries, except at the bottom boundary where either a slip or no-slip condition is applied. Initially, the fluid was at rest, and domain was stratified. The density variation across the interface was given by a smooth function, and the interface thickness was less than 0.05*H*. For the no-slip boundary condition, the vorticity at the bottom was modified based on the finite-difference analogue (Weinan & Liu (25)). The numerical domain was the same size as the experimental tank.

## 2.3 Experimental Conditions

The tank used was *L* = 182 cm long, 23 cm wide, and 30 cm deep. The total fluid height for each experiment was *H* = 20 cm and the gate was positioned at *L* = 30 cm from the end wall. The intrusions propagated about 5 lock lengths and were observed to travel at constant speeds after the initial acceleration from rest. The experiment was recorded using a CCD camera and VHS tapes, then analyzed using DigImage. DigImage is used to convert snapshot images of the experiment into time series images. The back of the tank was covered with tracing film and illuminated with two 95W fluorescent lamps.

The tank was first filled with a salt solution, with density $\rho_L$ and dyed with food coloring, to the required height, h. A layer of fresh water with density $\rho_U$ was added through a sponge float to reduce interfacial mixing until the total

height was reached. Then the gate was pushed down and the fluid behind the gate was stirred. To obtain the desired density $\rho_l$, salt was added to the lock, or solution was removed and replaced by an equal amount of fresh water. Food coloring was added to the solution in the lock. Densities were measured using an Anton Paar DMA 5000 density meter to a precision of $10^{-5}$ g/ml. The experiment started after pulling the lock gate vertically out of the tank.

The equilibrium intrusion case occurs when the gate is inserted and the two layers of fluid in the lock are well mixed so that the lock is filled with fluid of uniform density. The density of the lock fluid is then equal to the depth-weighted average density of the two layers. No salt is added to the lock and no solution is removed from the lock.

## 2.4 Results

An analytical model was developed by Cheong *et al*. (6), which predict the time-independent intrusion height, $h_U + h_L$, and speed $U$. The model further assumes that energy is conserved overall and dissipative effects due to viscosity are ignored.

The purpose of running these laboratory experiments was to add data to the previous experiments ran by Cheong *et al.* (6). The experiments were performed in the same way as Cheong *et al.* (6) and their theory and our laboratory experiments correspond very closely. The numerical solutions conducted by Flynn & Linden (8) are also comparable to the laboratory experiments that can be seen in Figure 2.3. Once released from the lock, the

gravity current propagates at approximately constant speed, $U_i$, over the field of view of the camera. This speed was measured from a horizontal time series (Figure 2.2) of the digitized experimental images (see Mehta *et al.*(15)). The non-dimensional velocity calculated by DigImage and the velocity calculated from the theory discussed in Cheong *et al.* (6) are very close (Table 1). There is a difference of less than 10% from the theory and calculated results from DigImage.

Figure 2.4 shows the intrusion speed (normalized by $\sqrt{g'_{LU}H}$) as a function of the non-dimensional interface height, $H_L / H$, for $h_E / H$. The thick black line indicates the speeds obtained form the global energy conserving model described in Cheong *et al.* (6), which proposes the following relationship between $U$, $H_L$, and $h_E$.

$$\frac{U}{\sqrt{g'_{LU}\,H}} = \tfrac{1}{2}\sqrt{\left(\frac{H_L}{H}\right)^2 - \frac{2H_L\,h_E}{H^2} + \frac{h_E}{H}}\,. \tag{2.14}$$

The model predicted by Cheong *et al.* (6) shows that the global minimum of $U = U_E$ when $H_L = h_E$ in which case there is no mass transport across the vertical level $z = H_L$ during the intrusion's gravitational adjustment. When $H_L \neq h_E$, the intrusion fluid steadily rises or falls behind the intrusion front, which provides an additional source of energy to drive the flow.

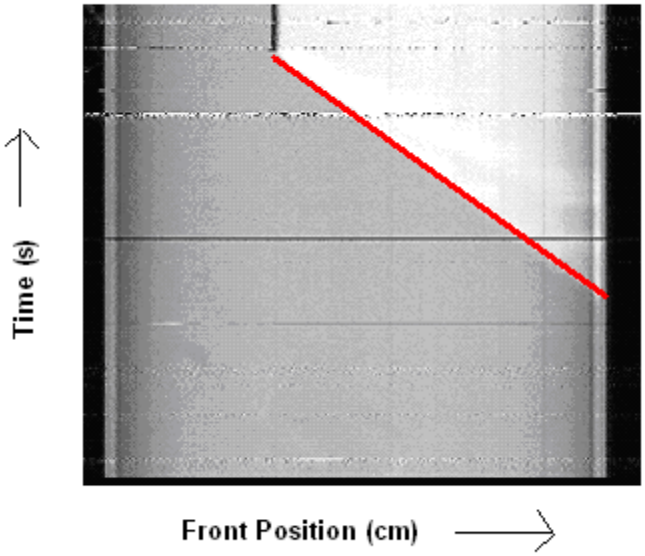


**FIGURE 2.2:** Example time series from an equilibrium experiment performed from DigImage. The interface between the shaded and unshaded region represents the cross-stream average density in the flow for every x and t. The red line indicates the interface and is an indication of the speed of the front.

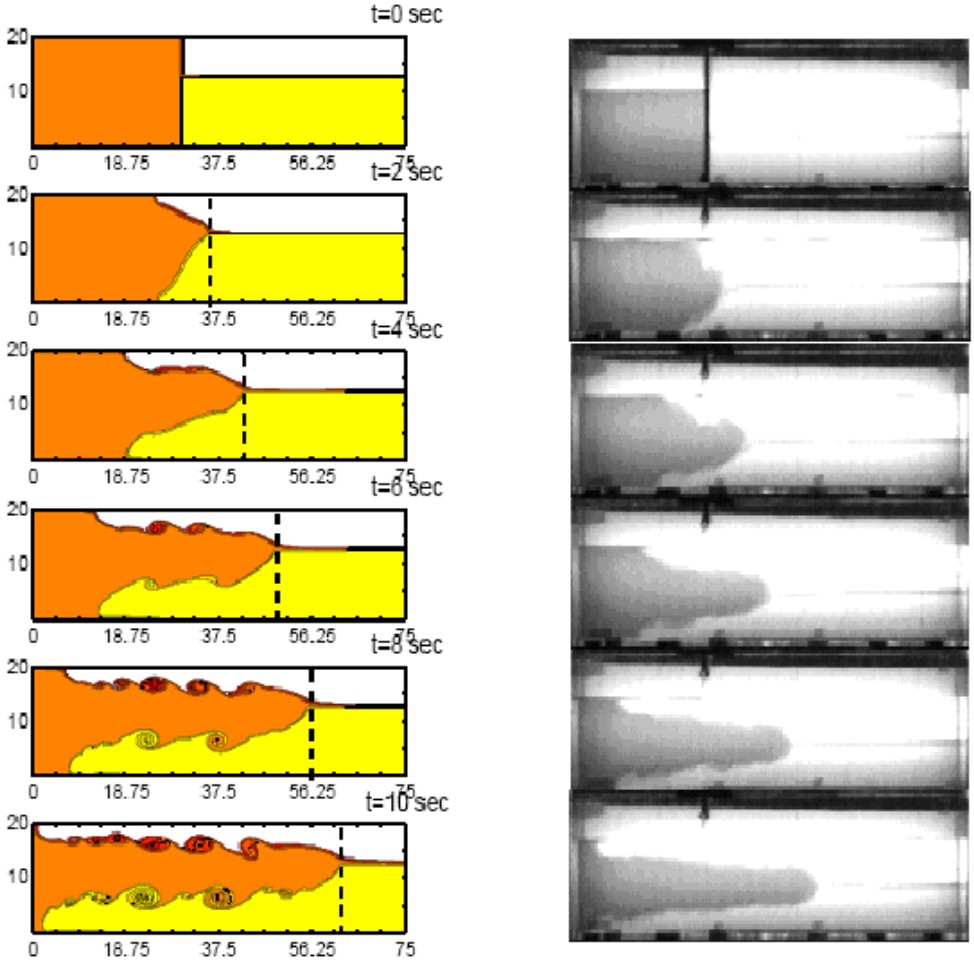


**FIGURE 2.3**: Image of an equilibrium IGC from the numerical solution from Flynn & Linden (8) (left); Image of an equilibrium IGC from laboratory experiments from DigImage (right).

**TABLE 2.1**: This table is the calculated data for the equilibrium intrusions from laboratory experiments and *U* theory comes from the theory discussed in Cheong *et al.* (6)

| Experiment | $\rho_L$ | $\rho_U$ | $\rho_0$ | $g'_{LU}$ | H (cm) | $H_L$ (cm) | $H_L/H$ |
|---|---|---|---|---|---|---|---|
| **A** | 1 1.019 | 0.998 | 1 | 20.738 | 20 | 9.836 | 0.492 |
| **B** | 1 1.020 | 0.998 | 1 | 21.504 | 20 | 10.126 | 0.506 |
| **C** | 1 1.020 | 0.998 | 1 | 21.327 | 20 | 9.998 | 0.500 |
| **D** | 1 1.021 | 0.998 | 1 | 21.935 | 20 | 10.000 | 0.500 |

| Experiment | $\rho_{Lock}$ | $h_E/H$ | $U_{theory}$ | $U_{calc}$ |
|---|---|---|---|---|
| **A** | 1.009 | .518 | 0.250 | 0.239 |
| **B** | 1.009 | .502 | 0.250 | 0.235 |
| **C** | 1.009 | .502 | 0.250 | 0.235 |
| **D** | 1.009 | .497 | 0.250 | 0.234 |

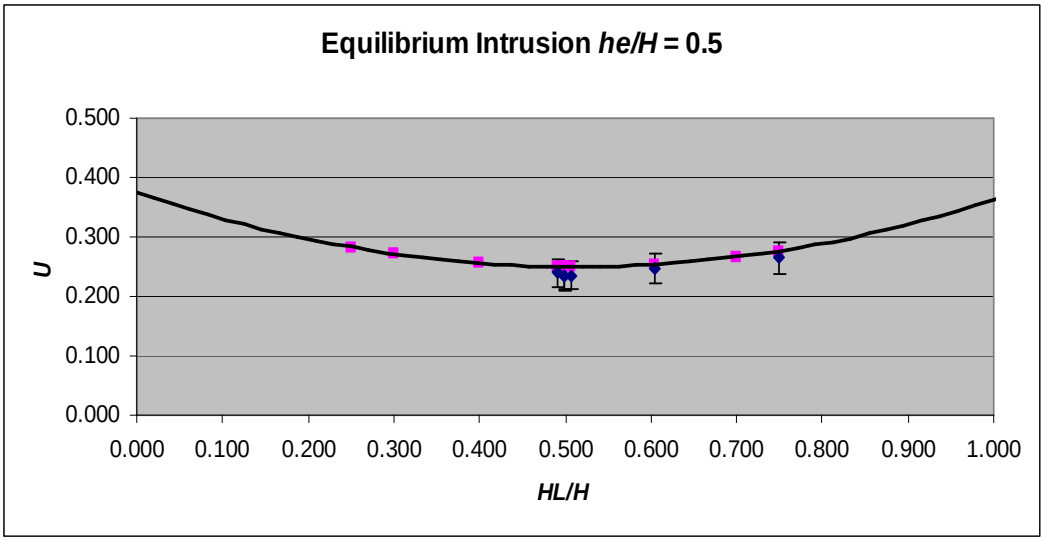


**FIGURE 2.4**: shows the intrusion speed (normalized by $\sqrt{(g'_{LU}H)}$ as a function of the non-dimensional interface height $H_L / H$. The thick solid black line indicates the theory developed by Cheong *et al.* (6). The blue diamonds indicate the laboratory experiments and the error bars are 10%.

## 2.5 Discussion and Conclusions

This chapter discussed the doubly symmetric intrusion in two layer fluids for which $H_U = H_L$ and $\rho_i = ½ (\rho_L + \rho_U)$. This intrusion can be considered as two gravity currents, one above and its mirror image below the interface. The doubly symmetric intrusion is considered an intrusion of density equal to the average density of the two layers propagating into two equal layers of depth. We extended the experiments to include equilibrium intrusions where the density is the depth weighted mean of the layer densities. We used a lock release setup where fluid of the depth weighted mean density intrudes into a two-layer stratification. The goal was to add my laboratory experiments to the

previous work done in Cheong *et al.* (6). The results from the equilibrium intrusions are close to the theory proposed by Cheong *et al.* (6). Cheong's model predicts a global minimum of $U = U_E$ when $H_L = h_E$ in which case there is no mass transport across the vertical level $z = H_L$ during the intrusion's gravitational adjustment. Looking at table 2.1, there is excellent agreement with Cheong's theory and the experiments conducted, both in the estimated speed of propagation, and the qualitative features of the flow (figure 2.3). The simulations show larger billows in the intrusive currents than are observed in the experiments, and this is due to the restriction to two dimensions in the calculations. In the equilibrium case, we can see that the interface ahead of the intrusion is flat.

# *Chapter 3*

## NON- EQUILIBRIUM INTRUSIONS IN TWO LAYER FLUIDS

### 3.1 Introduction

In general, most intrusions do not satisfy the equilibrium condition, i.e. $\rho_i \neq \rho_E$. In these non-equilibrium intrusions, the interface is deflected vertically by a wave that travels ahead of the intrusion and thereby changes the local upstream conditions. With these non-equilibrium intrusions, complications arise when describing this non-equilibrium flow. Unlike equilibrium flow, when $H_L \neq h_E$, the intrusion fluid steadily rises or falls behind the intrusion front, which provides an additional source of energy to drive the flow. We obtain experimental results that match closely with the energy balance analysis by Cheong *et al.* (6).

### 3.2 Control Volume Analysis

Experiments and numerical simulations of intrusive gravity currents are often conducted in channels of restricted spatial dimensions. In order to treat the intrusion and the wave, which in general travel at different speeds, the frame of reference is divided into two control volumes as illustrated in Figure 3.1. Control volume ABEF includes the intrusion at

rest. Control volume BCDE includes the nonlinear wave of amplitude *d*, which propagates upstream at a velocity $c - U > 0$ (in the shifted reference frame) (Flynn & Linden (8)).

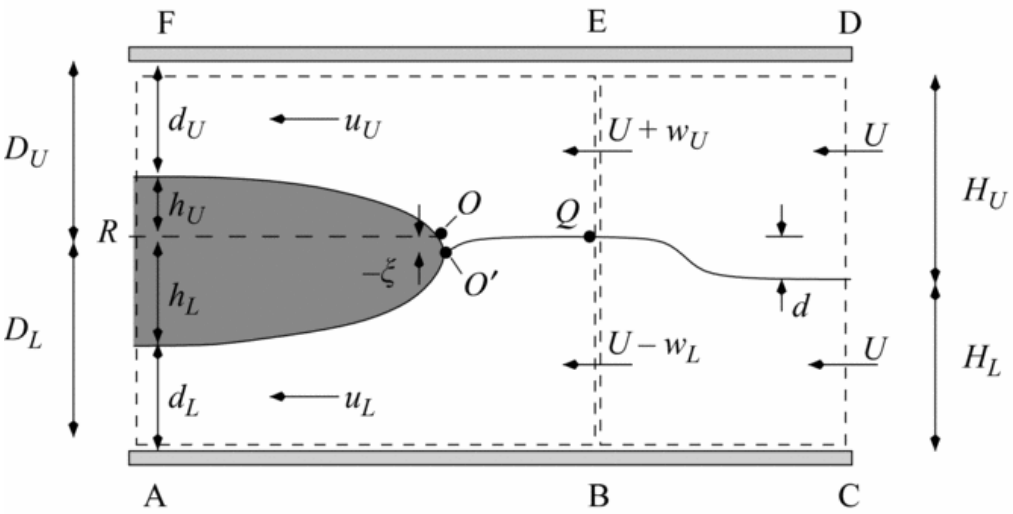


**FIGURE 3.1**: A non-equilibrium intrusion in a two-layer stratified media. The intrusion shown here has a density $\rho_I$ that is larger than $\rho_E$, the depth weighted mean density of the upper and lower layers. The leading wave therefore has a positive amplitude.

Due to wave-induced shear, the velocities of the upper and lower layers are different and are given, respectively by $U + w_U$ and $U - w_L$ where $w_U$ and $w_L$ denote perturbations to the uniform upstream flow field considered. This difference leads to an interfacial deflection $-\xi$ near the stagnation point *O*' where

$$\xi = \frac{(U + w_U)^2 - (U - w_L)^2}{2g'_{LU}}. \tag{3.1}$$

Although the flow is Boussinesq, this displacement will be appreciable if $\rho_I \neq \rho_E$. In general $|\xi|$ is not significantly less than $h_U$, $h_L$ and by Bernoulli's equation

$$u_U = \sqrt{2g'_{iU}\,(D_U - d_U + \xi)}\,, \quad u_L = \sqrt{2g'_{Li}\,(D_L - d_L - \xi)}\,, \tag{3.2}$$

where $D_U = H_U - d$ and $D_L = H_L + d$ denote, respectively, the perturbed upper and lower layer depths (figure 3.1). Using these results in the mass conservation equations for the upper and lower layer yields

$$U + u_U = \frac{d_U}{D_U}\sqrt{2g'_{iU}\,(D_U - d_U + \xi)}, \tag{3.3}$$

And

$$U - w_L = \frac{d_L}{D_L}\sqrt{2g'_{Li}(D_L - d_L - \xi)}, \tag{3.4}$$

respectively. By combining these results with (3.1), $\xi$ can be expressed entirely in terms of the distances $d_U$, $d_L$, $D_U$, and $D_L$ and the reduced gravities $g'_{IU}$. $g'_{LU}$, and $g'_{LI}$

$$\xi = \frac{\frac{g'_{iU}}{g'_{LU}}\,\frac{d_U^2}{D_U^2}\,(D_U - d_U) - \frac{g'_{Li}}{g'_{LU}}\,\frac{d_L^2}{D_L^2}(D_L - d_L)}{1 - \frac{g'_{iU}}{g'_{LU}}\,\frac{d_U^2}{D_U^2} - \frac{g'_{Li}}{g'_{LU}}\,\frac{d_L^2}{D_L^2}}. \tag{3.5}$$

Furthermore, taking the difference between (3.3) and (3.4) and eliminating the wave induced velocity $w_L$ of the lower layer, yields

$$\frac{w_U\,H}{D_L} = \frac{d_U}{D_U}\sqrt{2g'_{iU}(D_U - d_U + \xi)} - \frac{d_L}{D_L}\sqrt{2g'_{Li}\,(D_L - d_L - \xi)}. \tag{3.6}$$

Horizontal momentum is conserved in the control volume ABEF and following the same analysis, the following equation is obtained.

$$\frac{p_O - p_Q}{\rho_0} H = g'_{iU} \left\{ \frac{1}{2} \left( D_U^2 - d_U^2 \right) - \frac{2d_U}{D_U} (D_U - d_U)^2 \left[ 1 + \frac{\xi}{D_U - d_U} \right] \right\} + g'_{Li} \left\{ \frac{1}{2} \left( D_L^2 - d_L^2 \right) - \frac{2d_L}{D_L} (D_L - d_L)^2 \left[ 1 - \frac{\xi}{D_L - d_L} \right] \right\}. \tag{3.7}$$

Moreover, the pressure difference $p_O - p_Q$ can again be determined by applying Bernoulli's equation upstream along the interface whereby

$$\frac{p_O - p_Q}{\rho_0} = \frac{g'_{iU} g'_{Li}}{g'_{LU}} \left[ \frac{d_U^2}{D_U^2} (D_U - d_U + \xi) + \frac{d_L^2}{D_L^2} (D_L - d_L - \xi) \right]. \tag{3.8}$$

Combining 3.7 and 3.8 yields the momentum balance

$$\frac{H g'_{iU} g'_{Li}}{g'_{LU}} \left[ \frac{d_U^2}{D_U^2} (D_U - d_U - \xi) + \frac{d_L^2}{D_L^2} (D_L - d_L - \xi) \right] = g'_{iU} \left\{ \frac{1}{2} \left( D_U^2 - d_U^2 \right) - \frac{2d_U}{D_U} (D_U - d_U)^2 \left[ 1 + \frac{\xi}{D_U - d_U} \right] \right\} + g'_{Li} \left\{ \frac{1}{2} \left( D_L^2 - d_L^2 \right) - \frac{2d_L}{D_L} (D_L - d_L)^2 \left[ 1 - \frac{\xi}{D_L - d_L} \right] \right\}. \tag{3.9}$$

In the experiments performed for this thesis and previous experiments reported in Sutherland *et al.* (22) and Cheong *et al.* (6) show that the upstream wave may have an amplitude comparable to or greater than the upper or lower layer depth. In these experiments, the intrusion was generated by releasing intermediate density fluid from a lock by removing a vertical barrier. The amplitude of the wave can be estimated by considering the vertical adjustment of the intrusion fluid as it is release from the lock. When the density of the intrusion, $\rho_I$ exceeds the depth

weighted mean density $\rho_E$, the intrusion will sink relative to the upstream interface and consequently over an interval $\Delta t$, a volume of fluid

$$V = \Lambda(h_E - H_L)U\,\Delta t \tag{3.10}$$

is added to the lower layer. Here $h_E$ is the equilibrium height defined earlier (2.5) and $\Lambda$ is an unknown factor that we will use to characterize the collapse of the intrusion fluid towards its level of neutral buoyancy. If this adjustment is static, $\Lambda = 1$, but expected is a smaller value because dynamic effects are important. The addition of volume to the lower layer requires the dense fluid ahead of the intrusion to rise by

$$d = \frac{V}{(c-U)\Delta t} = \Lambda(h_E - H_L)\frac{U}{c-U}. \tag{3.11}$$

Experiments conducted by Cheong *et al.* (6) give a value of $\Lambda \approx 0.3$.

### 3.3 Experimental Conditions

The experimental conditions were similar to the equilibrium intrusion case. The tank used was $L$ = 182 cm long, 23 cm wide, and 30 cm deep. The total fluid height for each experiment was $H$= 20 cm (with the exception of one experiment at 16 cm) and the gate was positioned at $L$ = 30 cm from the end wall. The difference in the non-equilibrium intrusion case is that salt is added or lock fluid removed prior to lifting the gate. In experiments with $\varepsilon$ > 0, salt is added to the lock section of the tank, but not enough that it

exceeds the lower layer fluid density ($\rho_L$). In this paper, to characterize the relative density of the intrusion and the average density of the ambient, we use a parameter ε defined as

$$\varepsilon = \frac{\rho_I - \rho_{AVG}}{\Delta \rho} \tag{3.12}$$

where $\rho_{AVG} = (\rho_L + \rho_U)/2$ is the average density of the two layers and $\Delta \rho = \rho_L - \rho_U$, the density difference between the two layers. The values of $\varepsilon$ range from -0.5 for an intrusion density equal to the light top layer, to 0.5 for an intrusion density equal to the dense lower layer. Experiments with $\varepsilon < 0$ occur when lock fluid needs to be removed from the tank and fresh water is added. After the necessary density is established, the experiment continues like the equilibrium case. Values of $\rho_L$ were determined so that $-0.40 < \varepsilon < 0.40$.

**TABLE 3.1** : This table describes the non-equilibrium experiments performed.

| Experiment | $H$ (cm) | $H_L$ (cm) | $H_L/H$ (cm) | $\varepsilon$ | $\rho_L$ | $\rho_U$ | $\rho_0$ |
|---|---|---|---|---|---|---|---|
| **1** | 20.000 | 15.082 | 0.754 | 0.254 | 1.020 | 0.998 | 1.000 |
| **2** | 20.000 | 5.574 | 0.279 | -0.254 | 1.020 | 0.998 | 1.000 |
| **3** | 20.000 | 10.492 | 0.525 | 0.316 | 1.020 | 0.998 | 1.000 |
| **4** | 16.000 | 7.385 | 0.462 | -0.202 | 1.023 | 0.998 | 1.000 |
| **5** | 20.000 | 8.525 | 0.426 | 0.266 | 1.020 | 0.998 | 1.000 |
| **6** | 20.000 | 12.542 | 0.627 | 0.335 | 1.020 | 0.998 | 1.000 |
| **7** | 20.000 | 11.935 | 0.597 | -0.187 | 1.020 | 0.998 | 1.000 |
| **8** | 20.000 | 10.492 | 0.525 | 0.295 | 1.040 | 0.998 | 1.000 |
| **9** | 20.000 | 10.492 | 0.525 | -0.226 | 1.040 | 0.998 | 1.000 |
| **10** | 20.000 | 10.892 | 0.545 | 0.410 | 1.040 | 0.998 | 1.000 |
| **11** | 20.000 | 10.333 | 0.517 | -0.391 | 1.041 | 0.998 | 1.000 |
| **12** | 20.000 | 10.889 | 0.544 | 0.210 | 1.041 | 0.998 | 1.000 |
| **13** | 20.000 | 10.000 | 0.500 | -0.203 | 1.040 | 0.998 | 1.000 |
| **14** | 20.000 | 10.164 | 0.508 | -0.277 | 1.040 | 0.998 | 1.000 |
| **15** | 20.000 | 10.492 | 0.525 | 0.283 | 1.041 | 0.998 | 1.000 |

## 3.4 Results

From Figure 3.2, the time series from DigImage shows that the non-equilibrium intrusion flows at a constant speed until it reaches the end wall and then end wall effects occur that increase the speed of the intrusion. Figure 3.3 shows images taken from the experiments and the corresponding numerical simulations. Similar to the equilibrium intrusions, there is agreement with the laboratory experiments and the calculations. The speed of propagations are similar as well as the qualitative features of the flow. The larger billows in the numerical simulations are formed because of the two dimensions in the calculations. From the numerical simulations and laboratory experiments, we observe when the intrusion is less dense than the mean depth-weighted density, the IGC flows above the undisturbed interface height. The IGC flows below the undisturbed interface height when the intrusion is denser than the depth-weighted density.

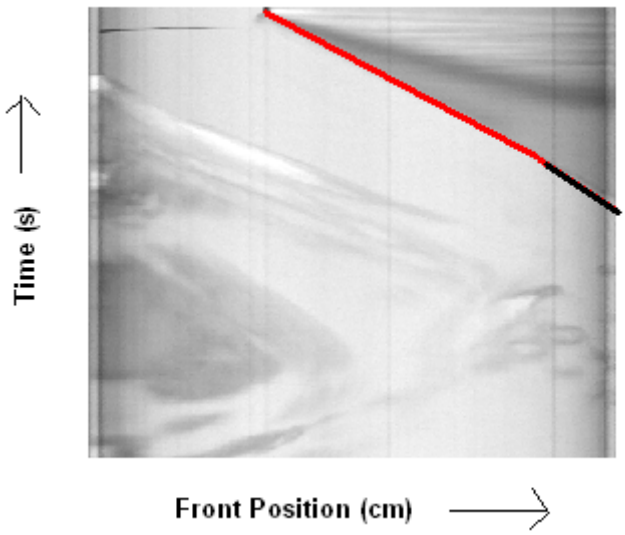


**FIGURE 3.2**: Time series of a laboratory non-equilibrium experiment where ε > 0. The red line is linear and therefore the speed can be assumed to be constant until it reaches the wall where the intrusion increases speed and is indicated by the black line.

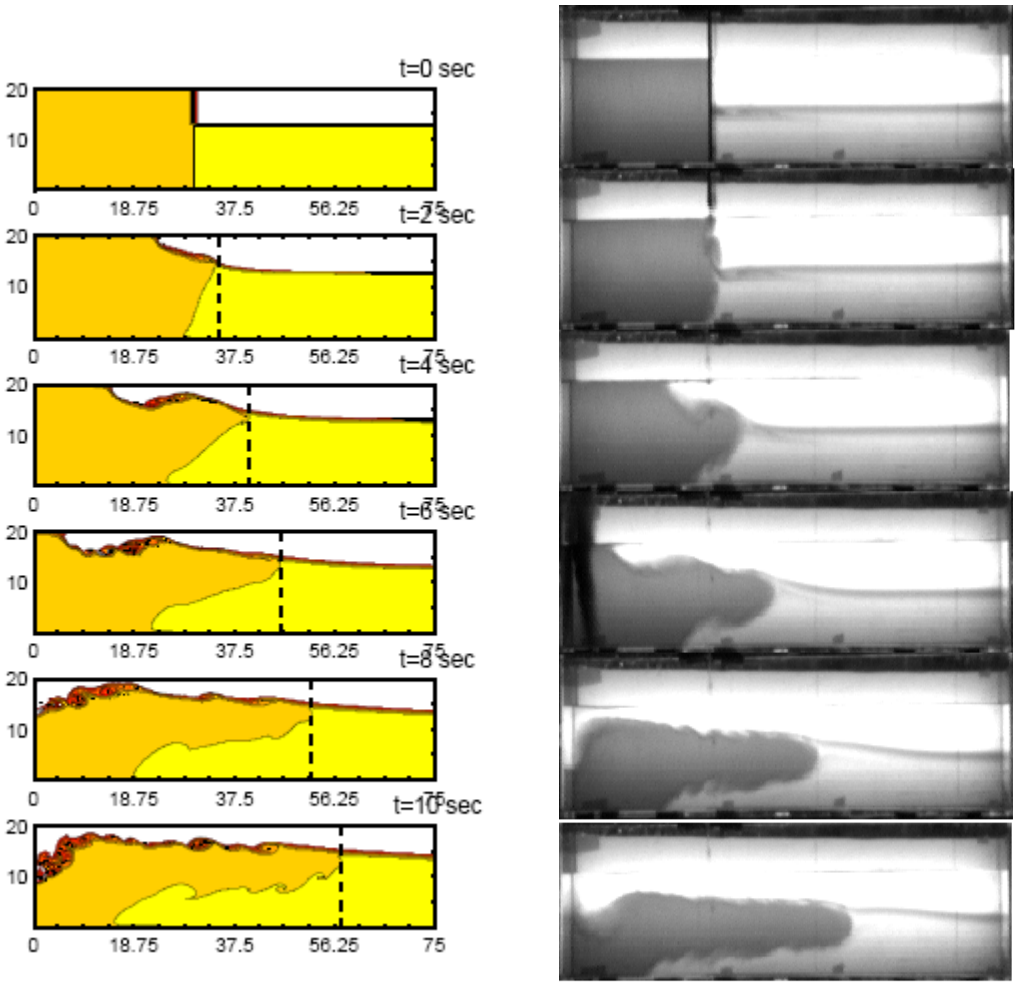


**FIGURE 3.3**: Image of a non-equilibrium IGC from a numerical simulation and experimental pictures.

As seen in Table 3.2, the non-dimensional velocity calculated by DigImage and calculated by conservation of mass, momentum, and energy are close. Figure 3.4 plots the dimensionless front speed *U,* against the dimensionless interface height. Solutions predicted by the energy conserving model described by Cheong *et al.* (6) are indicated by squares and experimental data is indicated by diamonds. The experimental error in the

front speed is about 10%. The energy model described by Cheong *et al.* proposes the following relationship between $U$, $H_L$, and $h_E$

$$\frac{U}{\sqrt{g'_{LU}\,H}} = \tfrac{1}{2}\sqrt{\left(\frac{H_L}{H}\right)^2 - \frac{2H_L\,h_E}{H^2} + \frac{h_E}{H}}\,. \tag{3.13}$$

**TABLE 3.2**: This table describes the calculations performed for the laboratory experiments.

| Experiment | $h_e$ (cm) | $h_e/H$ | $g'_{LU}$ | $\rho_{lock}$ | $u_{calc}$ | $U_{calc}$ | $U_{theory}$ |
|---|---|---|---|---|---|---|---|
| **1** | 15.073 | 0.754 | 21.582 | 1.015 | 4.137 | 0.199 | 0.215 |
| **2** | 4.917 | 0.246 | 21.866 | 1.004 | 3.889 | 0.186 | 0.216 |
| **3** | 16.312 | 0.816 | 21.795 | 1.016 | 4.85 | 0.232 | 0.242 |
| **4** | 4.774 | 0.298 | 24.069 | 1.006 | 4.336 | 0.221 | 0.243 |
| **5** | 15.321 | 0.766 | 21.092 | 1.015 | 5.299 | 0.258 | 0.271 |
| **6** | 16.705 | 0.835 | 21.236 | 1.016 | 4.311 | 0.209 | 0.213 |
| **7** | 6.260 | 0.313 | 21.092 | 1.005 | 4.837 | 0.235 | 0.272 |
| **8** | 15.891 | 0.795 | 41.102 | 1.031 | 6.127 | 0.214 | 0.243 |
| **9** | 5.477 | 0.274 | 41.163 | 1.01 | 6.123 | 0.213 | 0.256 |
| **10** | 18.195 | 0.910 | 40.986 | 1.036 | 5.742 | 0.201 | 0.232 |
| **11** | 2.183 | 0.109 | 41.889 | 1.003 | 8.039 | 0.278 | 0.257 |
| **12** | 14.194 | 0.710 | 41.716 | 1.028 | 6.403 | 0.222 | 0.242 |
| **13** | 5.940 | 0.297 | 41.153 | 1.011 | 6.519 | 0.227 | 0.25 |
| **14** | 4.462 | 0.223 | 41.319 | 1.008 | 6.22 | 0.216 | 0.252 |
| **15** | 15.670 | 0.783 | 41.820 | 1.032 | 6.156 | 0.213 | 0.243 |

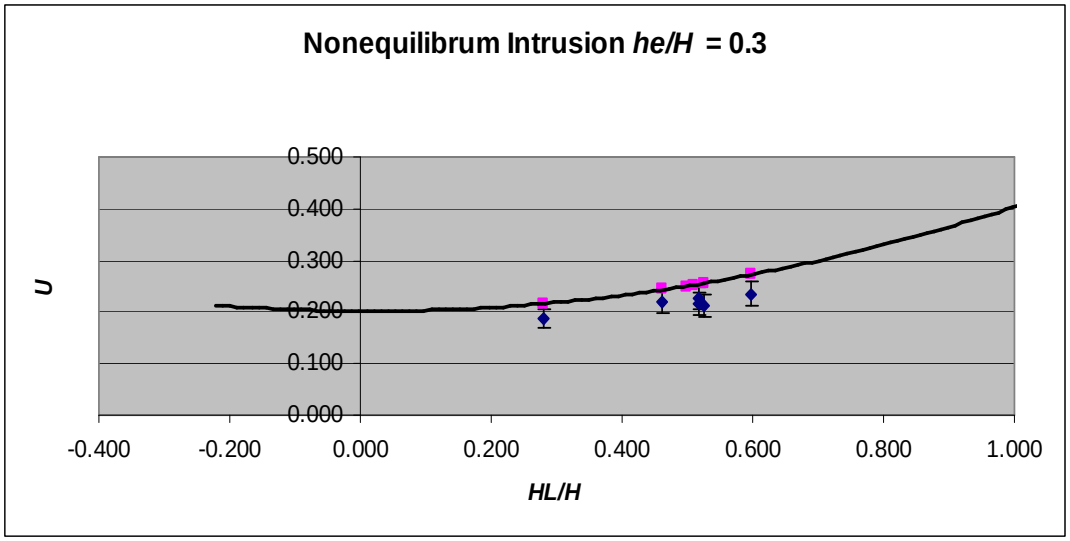


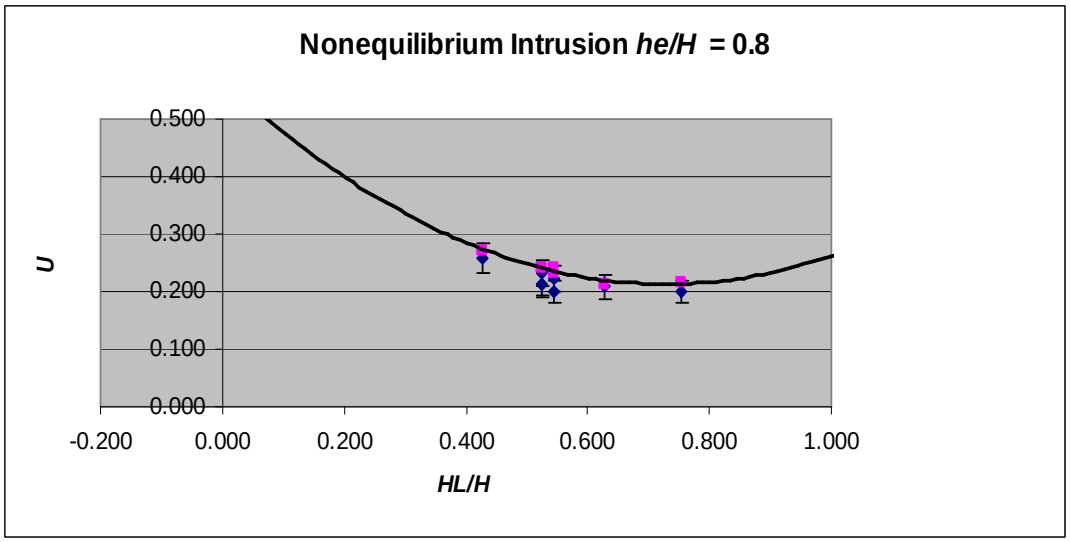


**FIGURE 3.4**: shows the relationship between theory and experimental values where the intrusion speed is normalized by $\sqrt{g'_{LU}H}$ as a function of the non-dimensional interface height, $H_L/H$. The diamonds are the experimental results and the error bars are 10%. The squares are a theoretical prediction from the numerical simulations. And the thick black line is equation 3.13.

## 3.5 Discussion and Conclusions

A fluid intrusion necessarily excites an upstream interfacial wave when the intrusion density, $\rho_I$, differs from the depth-weighted mean density, $\rho_E$, of the upper and lower layers. In general, this disturbance will be nonlinear and will exert some non-trivial dynamical influence in that the wave deflects the interface ahead of the intrusion and thereby alters the vertical position of the stagnation point, and causes a shear such that the local horizontal velocities of the upper and lower layers are non-equal. These effects may be incorporated into existing models by combining the shallow water equations with mass, momentum, and energy conservation applied to a control volume surrounding the intrusion head. For non-equilibrium flow, the center of mass of the intrusion may rise or fall some substantial vertical distance, which can lead to a wave excitation along the upstream interface.

This chapter discussed non-equilibrium intrusions in two layer fluids for which $H_U \neq H_L$. When a non-equilibrium intrusion occurs, the interface is either elevated or depressed by a long wave that propagates ahead of the IGC. This wave appears to be generated by the gravitational adjustment of the lock fluid when the gate is removed. Following Cheong *et al.*'s model and theory, we provided additional experiments of an IGC propagating along a sharp density interface at high Reynolds numbers.

Our experimental and numerical simulations results agree within ten percent.

# *Chapter 4*

# GRAVITY CURRENTS IN A CONTINUOUS STRATIFIED AMBIENT

## 4.1 Introduction

This chapter extends the work on intrusions in two-layer stratification, described in Chapter 3, to intrusions in a continuous stratification. While the principles behind this type of intrusion have many similarities with a current in two-layer stratification, there are some fundamental differences. In a continuously stratified ambient fluid, internal waves of a different nature to the interfacial waves in a two-layer system can be generated.

Experimental work on intrusions in a continuous stratification has been carried out from different vantage points. The earliest relevant experiments were conducted by Wu (26) who examined the release of a semicircular region at a rigid end wall, and Schooley & Hughes (18) who studied the flow generated by mixing a small but confined area in a stratification. Manins (13) carried out experiments with a continuous flux from a horizontal line source at an end wall of a channel. More recent experiments have investigated intrusions from a rectangular lock release at an end wall, of various depth ratios (Maxworthy *et al.* 14).

Kao (11, 12) and Barenblatt (1), among others, analyzed theoretically the propagation velocity of the intrusion formed by the collapse of a mixed region. They identified three stages of the intrusion. The initial stage is where the intrusion is formed and accelerates. Then there is a principal stage, where the driving buoyancy force is balanced by form and wave drag, and a final viscous stage, during which viscous forces affect the propagation of the thinned intrusion. The effects of the internal waves generated during the initial stage, described in detail by Wu (26), were further analyzed by Manins (13). Manins calculated the effects on the propagation velocity of the zero-frequency columnar internal wave modes and obtained a positive comparison with earlier experiments. Maxworthy *et al.* (14) observed that their lock-release intrusions generated internal solitary waves and they identify subcritical and supercritical regimes, where the gravity current travels faster or slower than the fastest internal wave. Some researchers believe that these waves can extract significant energy from the gravity current. The work by Cheong *et al.* (6), who assumed perfect conversion of potential energy into kinetic energy of the current, and by Flynn & Linden (8) who studied the kinematics of the interfacial wave, suggest that only a small amount of energy is extracted by the wave in the sharp interface case. This chapter will discuss if this is true for the continuously stratified case.

## 4.2 Internal Waves

One of the fundamental differences between the gravity currents in Chapter 3 and the present chapter is the presence of internal waves. To start the discussion of internal waves, we derive the equations for linear waves in a continuous density stratification. We first start with the Navier Stokes equations for an incompressible and inviscid fluid, representing conservation of mass, conservation of momentum, and incompressibility:

$$\nabla . \mathbf{U} = 0, \tag{4.1}$$

$$\rho \frac{D\mathbf{U}}{Dt} = -\nabla p + \rho \mathbf{g}, \tag{4.2}$$

$$\frac{D\rho}{Dt} = 0. \tag{4.3}$$

Here ***U***, $\rho$, and $p$ represent the velocity, density, and pressure of the fluid, respectively. In (4.2), the factor ***g*** in the forcing term represents the gravitational acceleration, which acts downwards along the z- axis. The material derivative is indicated by $D/Dt$. Small two dimensional disturbances in a fluid otherwise at rest (no mean velocity) are analyzed by substituting

$$\begin{aligned} \mathbf{U} &= (u, 0, w) \\ \rho &= \bar{\rho} + \rho' \\ p &= \bar{p} + p' \end{aligned} \tag{4.4}$$

With these substitutions, (4.1) to (4.3) can be linearized by discarding all second order perturbation terms. We make the Boussinesq approximation by neglecting the effect of the density perturbation on the inertial terms, and retain the effect of the density perturbation on the gravity term. The balance of the mean values is subtracted to obtain

$$\frac{\partial u}{\partial x}+\frac{\partial w}{\partial z}=0, \tag{4.5}$$

$$\bar{\rho}\frac{\partial u}{\partial t}=-\frac{\partial p'}{\partial x}, \tag{4.6a}$$

$$\bar{\rho}\frac{\partial w}{\partial t}=-\frac{\partial p'}{\partial z}-\rho' g, \tag{4.6b}$$

$$\frac{\partial}{\partial t}\rho'+w\frac{\partial}{\partial z}\bar{\rho}=0. \tag{4.7}$$

We can introduce a streamfunction $\Psi$ because of (4.5) that gives us

$$u=-\frac{\partial \psi}{\partial z}, \qquad w=\frac{\partial \psi}{\partial x}. \tag{4.8}$$

We substitute the streamfunction into (4.6) and (4.7) and (4.6a) can be differentiated with respect to z and (4.6b) with respect to x. Subtracting the resulting equations and combining with (4.7) yields

$$\frac{\partial}{\partial t}^2\left[\left(\frac{\partial}{\partial x}\right)^2+\left(\frac{\partial}{\partial z}\right)^2\right]\psi+N^2\left(\frac{\partial}{\partial x}\right)^2\psi=0, \tag{4.9}$$

where the buoyancy frequency $N$ is

$$N^2=-\frac{g}{\overline{\rho}}\frac{\partial\overline{\rho}}{\partial z}. \tag{4.10}$$

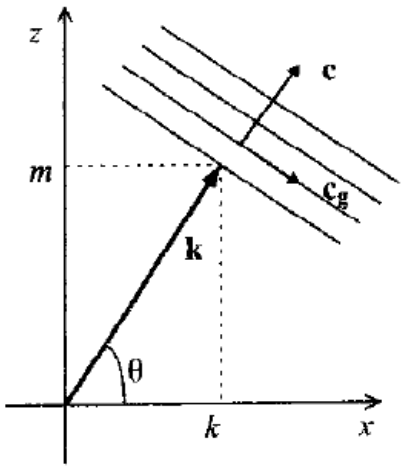


**FIGURE 4.1**: Sketch showing the wave vector, phase velocity, and group velocities of an internal wave.

In a vertically confined fluid the internal wave rays reflect off the top and bottom boundaries. The reflections combine to form a wave pattern in which the wave rays traveling up and down are impossible to tell apart. So it is then useful to look for horizontally traveling waves with a vertical amplitude dependence. So we seek disturbances of the form

$$\psi = \hat{\psi}(z)e^{ik(x-ct)}, \tag{4.11}$$

with a horizontal wave number $k$ and a phase velocity $c = \omega / k$.

Substituting (4.11) into (4.9) yields

$$\left(\frac{\partial}{\partial z}\right)^2 \hat{\psi} - + \left(\frac{N^2}{c^2} - k^2\right)\hat{\psi} = 0. \tag{4.12}$$

This differential equation has oscillatory solutions for $\Psi(z)$ if $|N/c| > |k|$, and exponentially decaying solutions otherwise. Imposing boundary conditions at the top and bottom will yield eigenfunctions $\Psi n\ (z)$ with corresponding phase velocities $c_n$. For rigid boundaries the vertical velocity w must vanish at the boundaries $z = 0$ and $z = H$. On substitution of (4.11) into (4.8), this gives $\Psi(0) = 0$ and $\Psi(H) = 0$. The eigenfunction solutions of (4.12) become

$$\hat{\psi}_n(z) = A \sin\left(\frac{n\pi}{H} z\right), \tag{4.13}$$

with phase velocities

$$c_n = \frac{N}{\sqrt{k^2 + \left|\frac{n\pi}{H}\right|^2}}. \tag{4.14}$$

The group velocity of these solutions is given by

$$c_{g,n} = \frac{d\omega}{dk} = \frac{N\left|\frac{n\pi}{H}\right|^{2}}{\left[k^{2} + \left(\frac{n\pi}{H}\right)^{2}\right]^{3/2}}. \tag{4.15}$$

In this vertically bounded domain the phase and group velocities have the same direction (for example horizontal).

An important set of the eigenfunctions are the columnar modes. These modes have an infinite wavelength and zero frequency: $k \rightarrow 0$. Equation (4.11) shows that the streamfunction $\Psi$ is then only a function of height $z$. The fluid moves on horizontal planes with a velocity profile $u_n\,(z)$. Using (4.8), the velocity profile can be derived from the streamfunction eigenfunctions $\Psi_n(z)$ defined by (4.13), which yields

$$u_n(z) = -\hat{u}_n \cos\left(\frac{n\pi}{H} z\right), \tag{4.16}$$

where $u_n$ represents the amplitude of columnar wave mode $n$. The motion is independent of time $t$ and independent of the length $x$ along the domain. The velocity profiles for the modes $n$ = 1, 2, and 3 are shown in figure 4.2.

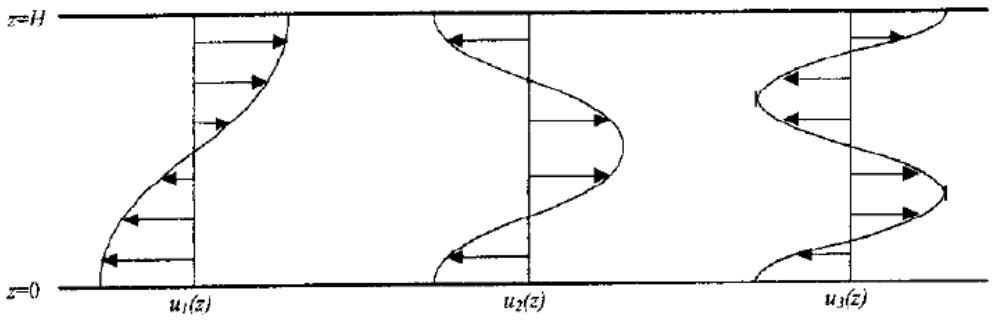


**FIGURE 4.2**: The vertical profiles of the horizontal velocity for the lowest three columnar modes.

Although these columnar modes do not have a horizontal variation, they will not always be present along the full length of the domain. An arbitrary disturbance will excite different columnar modes, and each of these will propagate away from the disturbance location at its own group velocity. Equations (4.14) and (4.15) show that for $k \rightarrow 0$ the phase velocity becomes equal to the group velocity, yielding

$$c_n = c_{g,n} = \frac{NH}{n\pi}. \tag{4.17}$$

At the front of each mode the streamfunction increases from zero to the profile $\Psi_n(z)$ over a finite region, and the horizontal velocity increases from zero to its final steady profile $u_n(z)$. McEwan & Baines (1974) showed that the width of the frontal region increases as $(Nt)^{1/3}$. Over this region there is a small vertical velocity $w$, which can be calculated from the horizontal

derivative of the streamfunction (4.8). This vertical velocity displaces the isopycnals vertically, resulting in a changed density profile after the front has passed, as shown in Figure 4.2 for mode $n = 1$. The change in the density profile can be calculated by integrating (4.7) across the frontal region, which gives us

$$\rho'(z) = \frac{\partial \overline{\rho}}{\partial z} \frac{\psi_n(z)}{c_{g,n}}. \tag{4.18}$$

If the domain is also horizontally confined there is an extra boundary condition that needs to be satisfied. For a rigid vertical end wall the horizontal velocity $u$ has to be zero, which gives with (4.8) that $\Psi = 0$. Equation (4.16) then shows that the amplitude $A$ of the reflected columnar wave is opposite to the amplitude of the incoming columnar wave. The reflected wave cancels out the streamfunction and the horizontal velocities of the incoming wave. However, the density perturbations of the incoming and reflected waves add up to leave a doubled net change in the density profile behind the front. This can be seen from (4.18), where both the group velocity and the streamfunction are of opposite sign for the reflected wave.

The linear wave analysis described above is based on the assumption of small disturbances that was made in (4.4). This means that the analysis only applies to the internal waves excited by the initial

propagation of an intrusion. With time, this small early disturbance may lead to finite horizontal displacements far ahead of the intrusion.

### 4.3 Theory

Intrusive gravity currents are created in the laboratory using a lock release as where the density of the intruding fluid on the left side of the lock, $\rho_I$, lies somewhere between the maximum and minimum densities, $\rho_L$ and $\rho_U$ respectively, on the right hand side of the gate. When the lock gate is removed, the fluid of density $\rho_I$ will travel along its level of zero buoyancy. In the special case where a gravity current propagates along the bottom boundary underneath fluid of lesser density the flow corresponds to a dense gravity current. Rottman & Simpson (17) and Maxworthy *et al.* (14) predict that in the early stages of a lock release the gravity current is observed to travel at a constant velocity, $U_0$, which from dimensional analysis takes the following form:

$$U_0 = F\sqrt{g'_{iref}H} \tag{4.19}$$

where $g'_{iref} = (\rho_{i} - \rho_{REF})/\rho_0$ is the reduced gravity of the IGC, $F$ is a Froude number, $\rho_0$ is a representative density and $\rho_{ref}$ is a reference density representative of the fluid into which the gravity current is intruding.

In the ideal energy conserving case Benjamin (2) showed that for the uniform density case $F$ = 0.5, which matches closely to experimental

measured values of $F$ = 0.48 from Shin, Dalziel, & Linden (19). Maxworthy *et al.* (14) and Ungarish (24) suggest values of $F$ somewhere between 0.25 and 0.266 for gravity currents in a stratified medium. The reason why the Froude number is different for the stratified and uniform cases is attributed to the fact that for the stratified case, the model assumes that the relevant density difference driving the current is $\rho_i - \rho_s$ ($z$ = ½ $h$), corresponding to the average ambient density over the depth of the current.

In lock experiments, IGCs form as a result of potential energy stored in the original lock configuration. From Cheong, *et al.* (6) we consider an energy model to predict the front speed of an intrusive gravity current into a continuously stratified medium. The available potential energy per unit area, $E$, due to the horizontal density difference, taking the level of zero buoyancy $h$ of the intrusion as the reference level, can be calculated as:

$$E = g\int_{-h_N}^{0}\Big(\rho_S(z') - \rho_i\Big)z'dz' + g\int_{0}^{H-h_N}\Big(\rho_i - \rho_S(z')\Big)z'dz',$$
$$= \frac{1}{3}\Big((\rho_L - \rho_i)gh_N^2 + (\rho_i - \rho_U)g(H-h_N)^2\Big).$$

(4.20)

If we define the equilibrium depth, $h_E$ as the depth of minimum potential energy, it is easy to show that this always occurs at half the height of the channel.

$$\frac{dE}{dh}\Big|_{h_N=h_E} = 0 \quad \Rightarrow \quad h_E = \frac{H}{2} \tag{4.21}$$

Since the minimum potential energy occurs at the mid height of the channel, we expect the slowest propagating IGC to always occur at this height, with maxima at the boundaries. Therefore we choose a quadratic form for the intrusion velocity,

$$U^2 = U_E^2\left(a\left(\frac{(h_N - h_E)}{H}\right)^2 + b\left(\frac{(h_N - h_E)}{H}\right) + c\right) \tag{4.22}$$

where $U$ is the speed of the intrusion, $U_E$ is the speed of the intrusion at the equilibrium height $h_E$, and $a$, $b$, and $c$, are the constant coefficients of the quadratic.

We assume that this system is Boussinesq, so we know from symmetry that the gravity current propagating along the top and bottom boundaries will travel at the same speeds. Therefore we can assume that $b = 0$. Also, we know that the velocity of the intrusion at the equilibrium height, $h_E$, is equal to the equilibrium speed $U_E$. Therefore, we can assume $c = 1$.

Using Maxworthy *et al.* (14), we can find the velocity of a bottom propagating current in a stratified medium.

$$U_{int}(h=0) = FNH \tag{4.23}$$

where *N*, defined in (4.10) is the buoyancy frequency of the stratified fluid. Additionally, the current at the mid depth, may be considered as two boundary propagating currents, traveling in a stratified medium of depth *H*/2. Since the buoyancy frequency of these layers is the same as the buoyancy frequency of the total system, the speed of the intrusion at the equilibrium height is

$$U_E = U_{int}(z=\frac{H}{2}) = FN\frac{H}{2}, \tag{4.24}$$

The IGC at the center height of the channel travels at exactly half the speed of the boundary propagating currents. Therefore

$$U = \frac{1}{2}FNH\left(12\left(\frac{h_N - \frac{H}{2}}{H}\right)^2 + 1\right)^{\frac{1}{2}}. \tag{4.25}$$

## 4.4 Experimental Conditions

The same tank was used for the continuous stratification and the two-layer experiments. To make the continuously stratified ambient fluid, the double bucket method was used. One bucket was filled with fresh water and the other was filled with salty water. The salty water was added

through the sponge float to fill up the experimental tank. As the experimental tank fills up to $H$= 20 cm, fresh water dilutes the salt water and a continuous stratification forms. (Referred to as the double tank method) The stratification was verified by using a conductivity probe. Every 5 cm, food coloring is added to the sponge float. After the gate is lowered, the lock fluid is mixed, and the experiment is recorded on a CCD camera and analyzed using Digiflow (Dalziel (7)).

We have also defined a variable $\zeta$, to compare the density of the intrusion with the density profile of the ambient fluid as:

$$\varsigma = \frac{\rho_i - \rho_U}{\rho_L - \rho_U} - 0.5 \, . \tag{4.26}$$

The experiment was started by pulling the gate vertically out of the tank. The flow images were captured. From this density field, the cross tank mean density, integrated vertically in the z-direction, was calculated for every x-position and time t. The front speed of the intrusive gravity current is calculated from the resulting *x, t* plot. See Figure 4.3 for an example time series of the experiments.

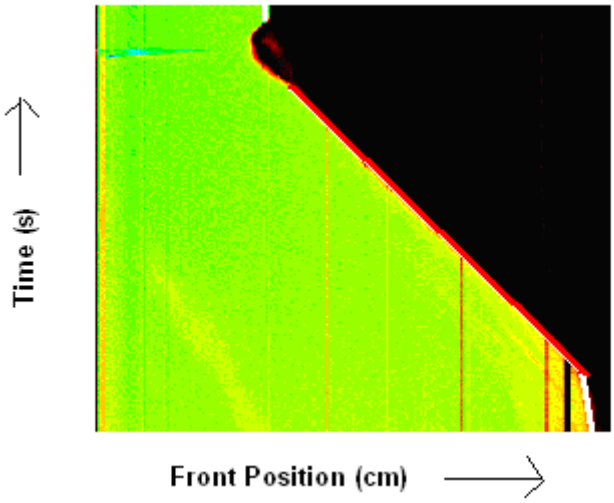


**FIGURE 4.3**: Time series of a continuous stratification. The red line is linear and therefore the speed can be assumed to be constant. The white line is where the intrusion changes speed as it reaches the end wall. This experiment is where $N$ = 1.036, $\zeta$ = 0.5, and $Fr$= 0.149.

## 4.5 Results

The experiments of the continuously stratified intrusions are compared to the numerical simulations conducted in Bolster *et al.* (3). Figure 4.4 shows images from the numerical solutions and the experiments. After an initial acceleration from rest, the intrusions were observed to travel at constant speeds until they reached the end of the tank. The results for the intrusion front speeds of the numerical simulations and experiments are shown and compared in Figure 4.6. Two curves are shown, corresponding to the theoretical results obtained in (4.25) for $F$ =

0.266 and 0.25. These two values are chosen from Maxworthy's *et al.* (14) experimental fit and Ungarish's (24) theoretical prediction.

The numerical results shown correspond nicely for the values of $N$ = 0.56 and 1 $s^{-1}$. Additionally, they agree well with the values predicted from (4.25), sitting between the two theoretical curves suggesting the energetic model presented here is accurate. The experimental results, while not as close in agreement with the theory as the numerical ones, compare favorably. The inconsistencies between the numerical and experimental data can possibly be attributed to the initial condition. In the experiments, the removal of the gate generates some vorticity and mixing between the lock and ambient fluid. This is not present in the numerical simulations and appears to affect the current in a very small way. This effect of the initial condition has been observed in previous gravity current experiments (ie: Patterson *et al.* (16)). There is also an observed asymmetry with currents in the upper half of the tank traveling slower than expected.

Internal gravity waves were generated in the experiments and numerical simulations (Figures 4.4 and 4.5). The wave speed for a long wave with vertical mode number $n$ is $U = NH / n \pi$. Therefore, all intrusions are subcritical with respect to mode 1 waves, subcritical to mode 2 waves for $0.27 < h_N < 0.73$ and supercritical to all higher modes, irrespective of $h_N$. The fluid ahead of the intrusion is deflected by mode 1 waves for all $h_N$ and mode 2 waves over a limited range of $h_N$ centered at mid-depth.

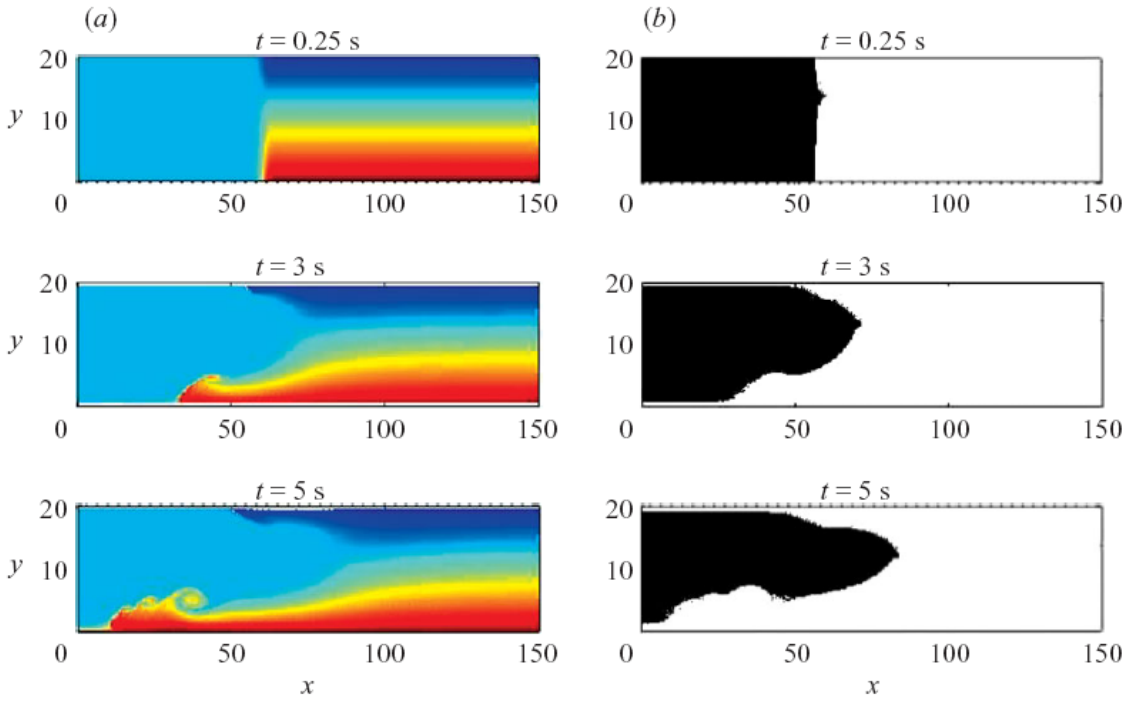


**FIGURE 4.4**: Image of an IGC in a continuous stratification from the numerical solution. The left hand column shows the stratified field with the darkest color corresponding to the lightest fluid. The right hand column shows the intrusion fluid in black.

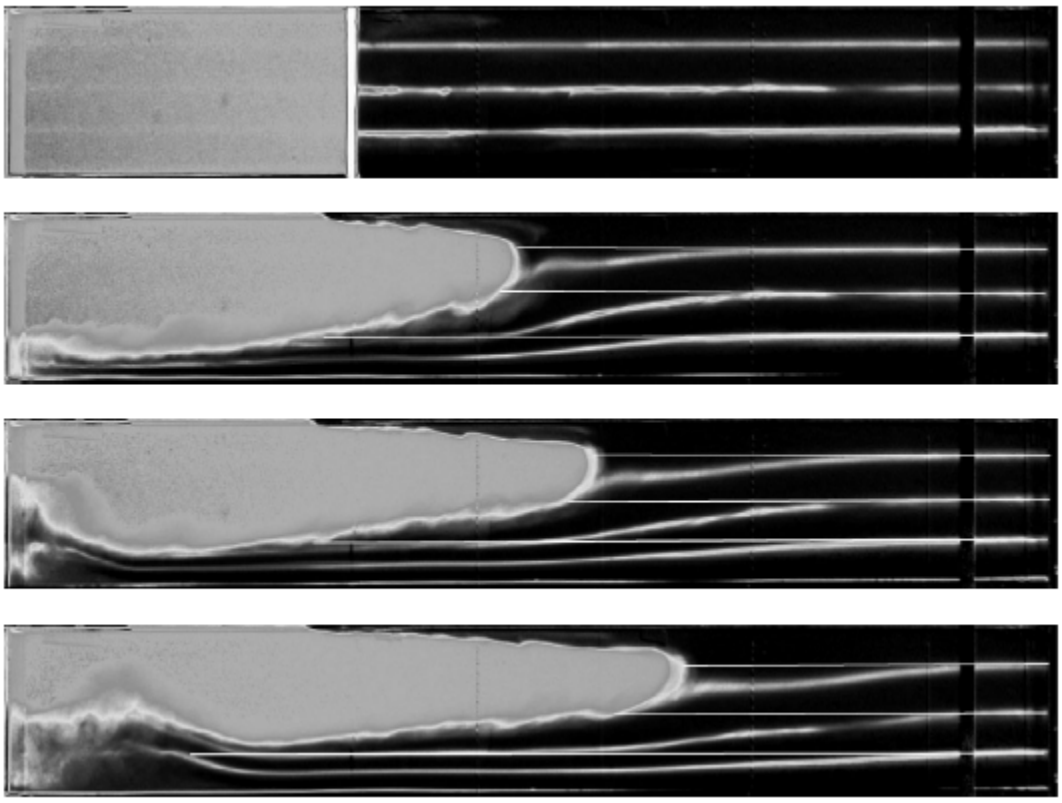

**FIGURE 4.5**: Image of an IGC in a continuous stratified field from laboratory experiments. In this case $N = 1$ and $h_N = 0.8$. Note that the isopycnal surfaces , marked with fluorescent dye, are deflected downwards ahead of the intrusion. They dye layers in the ambient are initially located at intervals of 5 cm.

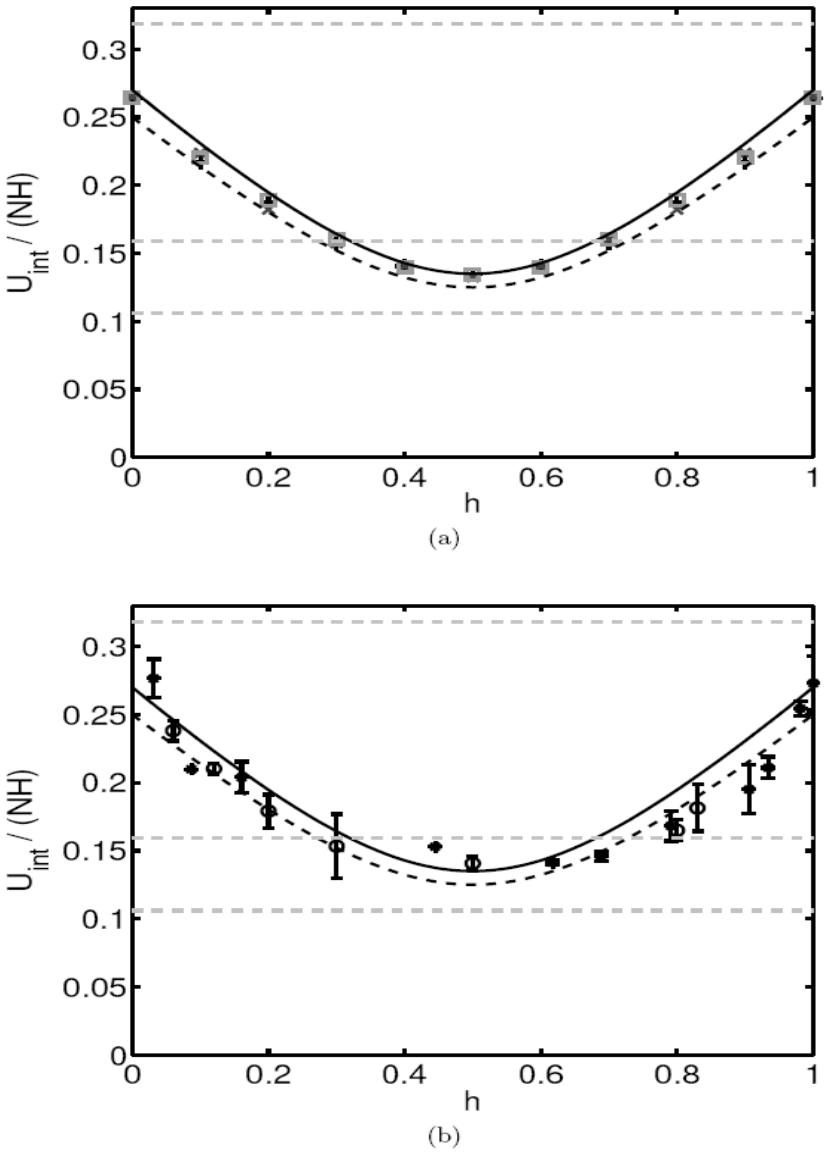


**FIGURE 4.6**: Comparison of dimensionless intrusion velocity ($U_{int}$ / NH) for (a) experiments and (b) numerical simulations to model predictions. Theory F = 0.266(-), F = 0.25 (--), Experiments (○($N^2$ =1$s^{-2}$),★ ($N^2$ = ¼ $s^{-2}$) and Numerical predictions ( x ($N^2$ = 1 $s^{-2}$), + ($N^2$ = ½ $s^{-2}$), □ ($N^2$ = ¼ $s^{-2}$)). The light grey horizontal dashed lines on each plot represent from top to bottom the first, second, and third mode long wave speed respectively.

We ran two sets of experiments where N= 0.56 and N=1 $s^{-1}$. During our experiments we observed that in the case $\varsigma = 0$ the intrusion propagated in the middle of the domain as expected. But when $\varsigma \neq 0$ so if $\varsigma > 0$ ($\varsigma < 0$) we observed a wave in front of the intrusion. Once the wave reflected by the end of the tank, the intrusion was forced to go up (down) in the middle of the domain as you can see on Figure 4.7. These internal gravity waves were generated in the laboratory experiments and numerical simulations (Figures 4.4 and 4.5). The wave speed for a long wave with vertical mode number $n$ is $U_w = NH / n\pi$ and these speeds are shown in figure 4.6 for $n$ = 1, 2, and 3. This shows that all intrusions are subcritical with respect to mode-1 waves, subcritical to mode-2 waves for $0.27 < h_N < 0.73$ and supercritical for all higher modes, irrespective of $h_N$.

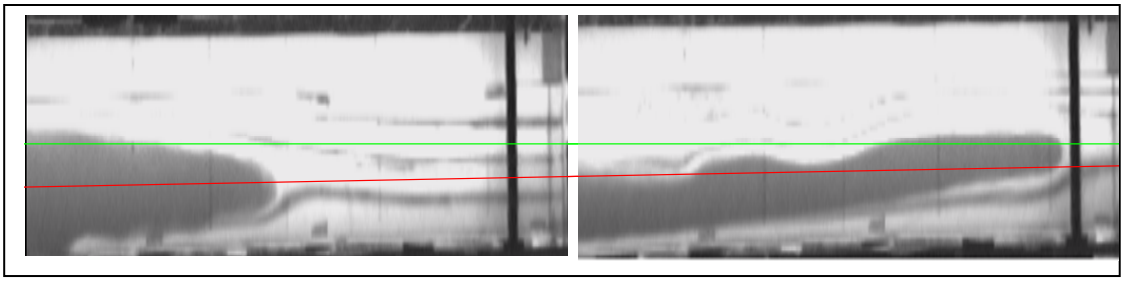

**FIGURE 4.7**: Displacement of the intrusion

We had also added some potassium permanganate to see the waves generated. When $\varsigma = 0$ the second mode is excising as on the figure 4.7. However when $\varsigma \neq 0$ it seems that the first mode is excising and then the second mode is also excised by the intrusion (Figure 4.8). But the

excitation occurs when the intrusion is moving in the middle of the domain as explained earlier. So we can think that the excitation of the second mode in this case is just an effect of the small tank (because after the reflection of the wave the intrusion is in the middle of the tank and we were back appreciatively at the case ς=0→second mode).

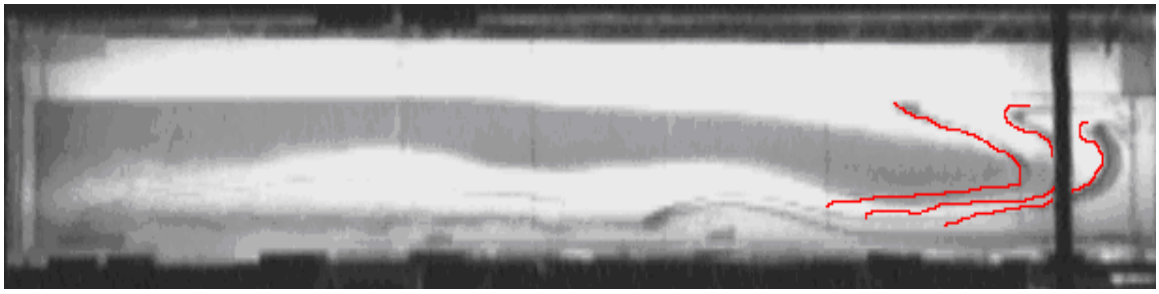

**FIGURE 4.8**: Permanganate (RED) shows the second mode excited.

**FIGURE 4.9**: The first mode is excited as shown in the red permanganate.

## 4.6 Discussion and Conclusions

In this chapter, we discussed Boussinesq intrusive gravity currents in a continuously stratified medium with constant buoyancy frequency *N*. The fluid intrudes at its height of neutral relative buoyancy. We used a

lock release setup where fluid of intermediate density intrudes into the stratified ambient. The goal of the experiments was to predict the front speed of the IGC during the initial phase. We compared an energy-conserving model to laboratory experiments and have shown that their values display close agreement to each other. The maximum velocities occur when the current travels along the top and bottom boundaries, with the minimum intrusion velocity occurring when the current travels at mid depth. The mid depth velocity is exactly half of the maximum velocity. In order to verify this, we conducted a full series of numerical and laboratory experiments. The measured intrusion velocities displayed good agreement with the values predicted by our model.

The results suggest that the role of internal gravity waves generated by the intrusion is small. Since the energy conserving theory provides an accurate estimate of the intrusion speed, this implies that the waves themselves carry little energy. A similar conclusion for the energy content of the interfacial wave for an IGC propagating in a two-layer fluid was drawn by Cheong, Kuenen, & Linden (6). The fact that the internal waves do not carry much energy does not mean that they do not play an important role in the flow. Flynn & Linden (8) modified Holyer & Huppert's (10) control volume analysis by including the wave changes to the upstream conditions and obtained accurate predictions for the intrusion speed.

The speed of a Boussinesq IGC propagating in an infinitely deep fluid is independent of the isopycnal surface the intrusion travels along, since in that case, the neutral buoyancy height has no meaning. Therefore, the change in speed with the neutral buoyancy height must be associated with the finite fluid depth. A similar deflection of the interface ahead of the IGC occurs in both the two-layer stratification and the continuous stratification case. All intrusions are subcritical to mode 1 waves and some intrusions are subcritical to mode 2 waves. The deflections that occur are asymmetrical about the mid-depth of the channel and need to be included in a control-volume analysis similar to the two-layer stratification can be used for the continuous stratification.

# *Chapter 5*

## CONCLUSION

Intrusive gravity currents are an important category of environmental flows. Chapters 2 and 3 discussed equilibrium and non-equilibrium intrusions in two layer stratifications with numerical and presented new laboratory experiments. Chapter 2 discussed doubly-symmetric intrusions in two layer fluids for which $H_U = H_L$ and $\rho_i = ½ (\rho_L + \rho_U)$ and equilibrium intrusions where the density of the intrusion is the depth-weighted mean of the two layers. The results from the laboratory experiments performed were compared to the theory proposed by Cheong *et al* (6). It was shown that there was excellent agreement between their theory and the new experimental data. Chapter 3 discussed non-equilibrium intrusions in two layer fluids. It was observed during laboratory experiments that an upstream interfacial wave occurs when the intrusion density, $\rho_I$, differs from the depth-weighted mean density, $\rho_E$, of the upper and lower layers. This wave appears to be generated by the gravitational adjustment of the lock fluid when the gate is removed. Our experimental and numerical simulations results agree within ten percent.

Chapter 4 discussed intrusions in a continuously stratified medium with constant buoyancy frequency $N$. The fluid intrudes at its height of neutral relative buoyancy. A model was developed based on energy

arguments and showed that the maximum velocities occur when the current travels at the top and bottom boundaries. The numerical and laboratory experiments were in good agreement with the values predicted by our model.

## BIBLIOGRAPHY

(1) G. Barenblatt. Dynamics of turbulent patches and intrusions in a stably stratified fluid. *Bull. USSR Acad. Sci. Ser. Atmos. Ocean Phys.* **14**(2), 195–206, 1978.

(2) T. B. Benjamin. Gravity currents and related phenomena. *J. Fluid Mechanics,* 31:209- 248, 1968.

(3) D. Bolster, A. Hang, & P.F. Linden. The front speed of intrusions into a continuously stratified medium. *J. Fluid Mechanics,* 594: 369-377, 2007.

(4) E. Becker and G. Schmitz. Energy deposition and turbulent dissipation owing to gravity waves in the mesospher. *J. Atmos. Sci.* 59, 54-68, 2002.

(5) R. E. Britter and J. E. Simpson. A note on the structure of the head of an intrusive gravity current. *J. Fluid Mechanics*, 112: 459-466, 1981.

(6) H.B. Cheong, J.J.P. Kuenen, & P. F. Linden. The front speed of intrusive gravity currents. *J. Fluid Mechanics*, 552:1-11, 2006.

(7) S.B. Dalziel. Digiflow User manual. http://www.damtp.com.ac.uk/lab/digiflow 2004.

(8) M.R. Flynn and P.F. Linden. Intrusive gravity currents. *J. Fluid Mechanics,* 568:193-202, 2006.

(9) D. C. Fritts and G.D. Nastrom. Sources of mesoscale variability of gravity waves. Part II: Frontal, convective, and jet stream excitation. *J. Atmos. Sci.* 49, 111-127, 1992.

(10) J. Y. Holyer and H. E. Huppert. Gravity currents entering a two-layer fluid. *J. Fluid Mechanics,* 100:739-767, 1980.

(11) T.W. Kao. Principal stage of wake collapse in a stratified fluid: two-dimensional theory. *Phys. Fluids*., 19, 1071-1074, 1976.

(12) T.W. Kao. Density currents and their applications. *J. Hydraul. Diw. ASCE.* 103 (HYB), 543-555, 1977.

(13) P.C. Manins. Intrusion into a stratified media. *J. Fluid Mechanics,* 74: 547-560, 1976.

(14) T. Maxworthy, J. Leilich, J. Simpson, and E.H. Meiburg. The propagation of a gravity current in a linearly stratified fluid. *J. Fluid Mechanics,* 453: 371-394, 2002.

(15) A. Mehta, B.R. Sutherland, & P.J. Kyba. Interfacial gravity currents: Part II-wave excitation. *Phys. Fluids*, 14:3558-3569, 2002.

(16) M.D. Patterson, J.E Simpson, S.B. Dalziel, & G.J.F. van, Heijst. Vortical motion in the head of an axisymmetric gravity current. *Physics of Fluid.,* 18, 86-97, 2006.

(17) J.W. Rottman and J.E. Simpson. The formation of internal bores in the atmosphere: A laboratory model. *Q. J. R. Metl. Soc.* 115, 941-963, 1989.

(18) A.H. Schooley and B.A. Hughes. An experimental and theoretical study of internal waves generated by the collapse of a two-dimensional mixed region in a density gradient. *J. Fluid Mechanics,* 51:159-175, 1972.

(19) J.O. Shin, S.B. Dalziel, & P.F. Linden. Gravity currents produced by lock exchange. *J. Fluid Mechanics*. 521, 1-34, 2004.

(20) J. E. Simpson. *Gravity currents in the Environment and the Laboratory*. Ellis Horwood. Chichester, 1987.

(21) J. E. Simpson. *Gravity Currents.* Cambridge University Press, Cambridge, England, 2nd edition, 1997.

(22) B.R. Sutherland, P.J. Kyba, & M.R. Flynn. Intrusive gravity currents in two-layer fluids. *J. Fluid Mechanics,* 514: 327-353, 2004.

(23) M. Ungarish and H.E. Huppert. On gravity currents propagating at the base of a stratified fluid. *J. Fluid Mechanics,* 458:283-301, 2002.

(24) M. Ungarish and H.E. Huppert. Energy balances for propagating gravity currents: homogenous and stratified ambients. *J. Fluid Mechanics,* 565, 363-380, 2006.

(25) E. Weinan and J.-G. Liu. Vorticity boundary condition and related issues for finite difference schemes. *J. Comput. Phys.* 124 (2), 368-382, 1996.

(26) J. Wu. Mixed region collapse with internal wave generation in a density stratified medium. *J. Fluid Mechanics,* 35: 531-544, 1969.